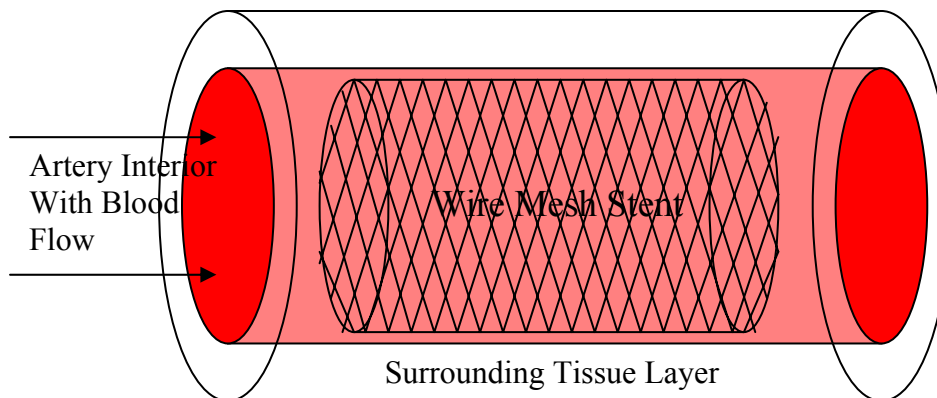


## Magnetic Resonance Induced Heating in a Vascular Stent

Ankur Chaudhury  
Siddharth Khasnavis  
Matthew Russell  
Vijay Sarathy



BEE 453: Computer Aided Engineering  
Ashim K. Datta  
Spring 2007

## Contents

[1] Executive Summary.....	3
[2] Introduction and Design Objectives.....	4-7
2.1 Background.....	4-5
2.2 Problem Schematic.....	5
2.3 Modeling.....	6
2.4 Design Objectives.....	6-7
[3] Results and Discussion.....	7-13
3.1 Results.....	7-11
3.2 Sensitivity Analysis.....	11-12
3.3 Results Compared with Expected Results.....	13
[4] Conclusion and Design Recommendations.....	13-14
4.1 Conclusion.....	13
4.2 Realistic Constraints.....	13-14
4.3 Design Recommendations.....	14
[5] Appendices.....	15-24
Appendix A – Model Physics.....	15-17
A.1 Geometry and Schematic.....	15
A.2 Governing Equations.....	15
A.3 Boundary and Initial Conditions.....	16
A.4 Meshes Used.....	17
Appendix B – Solution Details and Model Reports.....	17-21
B.1 Model Properties.....	18
B.2 Constants.....	19-20
B.3 Geometry type and Application Modes.....	20-21
Appendix C – Further Modeling.....	22-23
Appendix C – References.....	24-25

## **1. Executive Summary**

It is standard hospital practice to remove metallic objects from patients prior to MRIs. Since magnetic resonance imaging employs changing magnetic fields, even everyday items such as jewelry or keys run the risk of overheating due to induced currents leading to Joule heating. A potential problem arises, however, when the metal is subcutaneously located in the form of a medical implant. The present study evaluated this scenario by using finite element analysis to model a vascular stent under the influence of a standard MRI field. COMSOL Multiphysics software was used to conduct finite element analysis on two different stent sizes, each in the presence and absence of blood flow. The stents were modeled as stainless steel (type 316L) with internal diameters of 5mm and 8mm, length of 40mm, and wall thicknesses of 0.18mm and 0.22mm. The tests revealed that under the influence of blood cooling, the stents modeled did not overheat or cause arterial damage. Specifically, the large stent resulted in a maximum temperature of 310.807 K and the smaller stent led to 310.230 K, each after 30 minutes of heating. In the unrealistic absence of blood flow, the large and small stents reached maximum temperatures of 318.851 K and 312.297 K respectively. Ultimately, given variance in blood flow the true solutions lie somewhere in between the blood perfusion and static flow models.

## 2. Introduction and Design Objectives

### 2.1 Background

Medical implants can pose a danger to patients who are exposed to large magnetic fields such as those used in magnetic resonance imaging (MRI). Since most implants are not ferromagnetic, this danger is not primarily due to implants moving within a patient. Rather, it is the induced eddy currents within conductive implants which results in Joule heating and potential tissue damage.<sup>1,3,4,6,7,8,10</sup> A common type of conductive implant is a wire mesh stent used to expand and scaffold narrowing arteries. By far the most common applications of stents is in treatment of coronary artery disease, the leading cause of death in the United States.

Coronary artery disease involves plaque build up in the vessels perfusing the heart itself. This restriction of blood flow initiates death or injury of heart tissue and eventually leads to angina and heart attacks. The obstruction is predominantly removed using balloon angioplasty, which expands the affected artery and pushes plaque towards the artery walls. Consequently, a wire mesh stent is placed at the site and holds the artery open after surgery. Even after this procedure, scar tissue and plaque buildup can occur around the wire mesh and within the lumen of the stent, thus recapitulating the disease. This is known as restenosis. Given the high occurrence of restenosis in patients, it is desirable to monitor the coronary arteries post surgery with magnetic resonance imaging (MRI). However, prior to imaging it is important to evaluate the safety of MRI on patients with implanted stents.

The functioning of an MRI depends on the manipulation of atomic particles with magnetic fields. A 1.5 Tesla clinical MRI scanner, typically found in hospitals, applies a strong (1.5T) constant magnetic field to a patient and aligns the hydrogen nuclei in the volume being imaged. A homogeneous radio frequency (RF) magnetic field is then applied in pulses at the Larmor frequency (63.855 MHz for a 1.5T machine)<sup>16</sup> which is the frequency of precession of the hydrogen nuclei about the permanent magnetic field vector. This RF field is absorbed by the nuclei and causes a small fraction of them to align anti-parallel to the permanent field. When a RF field pulse ceases, the nuclei realign parallel to the permanent field and release a RF signal. Through the use of magnetic gradients, it is possible to map these weak signals to specific volume elements and create an image.<sup>16</sup> The permanent magnetic field is actually incapable of inducing a current in a metallic implant and instead the RF field, sometimes called the  $B_1$  field, is of interest to us. This field can reach a maximum amplitude of  $20\mu\text{T}$  in a typical 1.5T MRI machine and is pulsed in 1ms intervals with 10-100ms between pulses.<sup>2,5,15</sup>

The FDA provides guidelines that an implanted medical device must satisfy in order to be considered MRI safe.<sup>16</sup> These include a requirement that any medical device must not present any increased risk to personnel or patients when used in an MR environment. Because the primary safety concern for a stent in MRI is heating, we used computer

modeling to simulate the process in an implanted stent. Given that irreversible tissue damage occurs at temperatures greater than 45°C (318K), it is desirable that the tissue surrounding a stent remain below this critical temperature during an MRI procedure.

## 2.2 Problem Schematic

To develop a reliable understanding of MRI induced heating, we considered a few different models for this problem. In all models, we assumed that the stent was positioned with its axis parallel to the RF field, which resulted in maximum heating of the stent. In this case, the volumetric heating of the stent was calculated using a composite of Faraday's law and Joule heating. This value is given in Equation 1.<sup>7, 15</sup>

$$Q_{volume} = (\pi R_{stent} f B_1)^2 \phi t_f \sigma_{stent} \quad \text{(Equation 1)}$$

The stent is modeled as a thin cylindrical shell.

$R_{stent}$  = radius of the stent

$f$  = frequency of the RF field

$B_1$  = magnitude of the RF field

$\phi$  = fraction of the surface area of the cylindrical shell that is wire mesh

$t_f$  = fraction of the total time that the RF field is applied

$\sigma_{stent}$  = electrical conductivity of the stent.<sup>7, 15</sup>

Having determined a way to approximate stent heating, we moved to test two different geometries representing large and a small diameter coronary stents. The following table summarizes the dimensions of the two sizes of stent that were modeled:

**Table 1.** Dimensions of a small and large wire mesh stent.<sup>1</sup>

	Diameter (mm)	Length (mm)	Thickness (mm)
Small Stent	5	40	0.18
Large Stent	8	40	0.22

We modeled the stents as thin cylindrical shells placed on the artery wall. Knowing that the cooling effects of blood flow played a large role in heat removal, we modeled each stent with and without blood flow. This created a “best case” scenario where blood flow was unobstructed and a “worst case” scenario where blood flow was completely obstructed. In the two models with blood flow, the dynamic viscosity of blood was set at 0.003 Pa\*s and a value of 0.15m/s was used as the average velocity of blood.<sup>12, 17</sup> This constant velocity is an average diastolic velocity of blood flow in the coronary arteries taken from literature and actually represents a safety factor in our models (the actual average blood velocity should be higher, resulting in decreased heating). We also chose to apply the RF field for a 1/10 fraction of the total time of simulation, which is at the high end of the range of application in a clinical MRI procedure. This results in greater heating and established an additional safety factor.<sup>15</sup> The values of all other material properties and constants used in our models may be found in Appendix B.<sup>11</sup>

## 2.3 Modeling

We produced four computer models using the COMSOL multiphysics platform. These included both small and large stents with and without blood perfusion. An axis-symmetric geometry was used in all four models and consisted of artery, stent, and tissue subdomains. Figure 1 depicts the type of geometry used and when rotated about the Z axis, provides a three dimensional image of the realistic system. A more precise geometry is outlined in Appendix A.

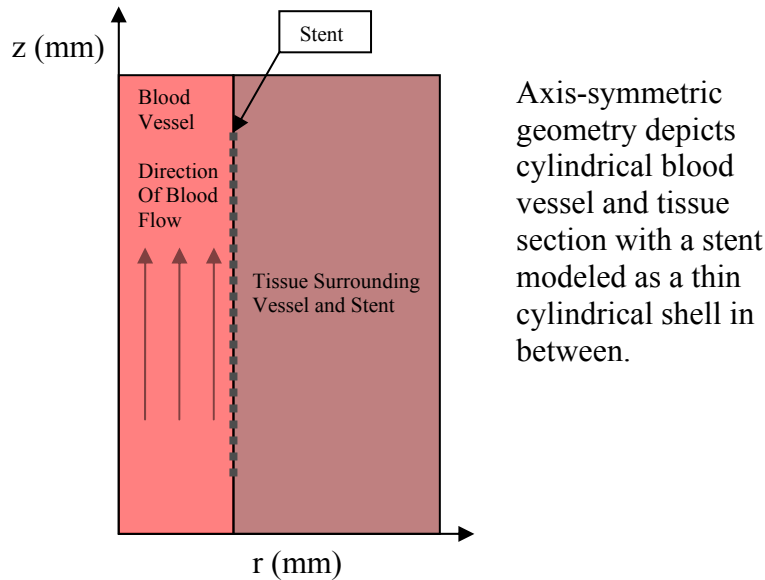


**Figure 1.** Schematic of implanted stent with axi-symmetric geometry.

These models accounted for heat conduction and convection away from the stents as well as fluid flow within the arterial lumen (in the perfusion trials). In addition to material properties and constants found in Appendix B, the governing equations, boundary conditions, initial conditions, and meshes used in our models may be found in Appendix A. All four models were sufficiently large so that the blood flow in the artery could become fully developed before reaching the stents and heat flow did not reach the outer boundaries of arterial tissue. This latter semi-infinite approximation was depicted by zero heat flux boundary conditions used on the right, top, and bottom boundaries of the tissue regions (Appendix A).

## 2.4 Design Objectives

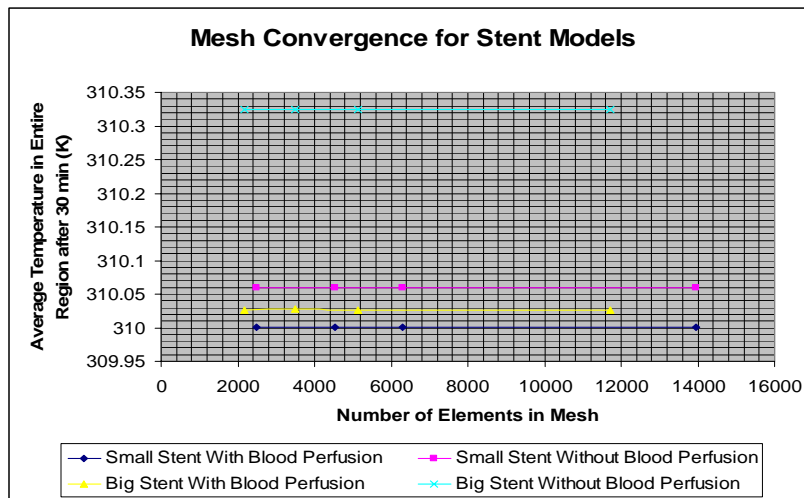
We aimed to develop an accurate model for the RF heating of an implanted wire mesh stent during an MRI procedure. Our goal was to use this model to determine whether a 1.5T clinical MRI procedure, typically used in hospitals, poses any danger to a patient with an implanted 316L steel stent. Therefore, we looked at the maximum temperatures

reached within the model geometries after simulation of a 30 minute MRI procedure and compared the results with the 45°C (318K) required for tissue damage. Additionally, we tested our models' sensitivity to variation in material properties and changes blood perfusion rates. This latter consideration was well examined through models without blood flow and helped us understand the effects of restenosis.

### 3. Results and Discussion

#### 3.1 Results

Each of our four models was first tested with different meshes to confirm the convergence of solutions. As a test statistic, we used the average temperature over the entire region of each model. Next, we varied the number of elements in each model by refining the mesh and re-solved. Figure 14 shows a graph of the average temperature in each model after 30 minutes of heating over the number of elements in the model's mesh.



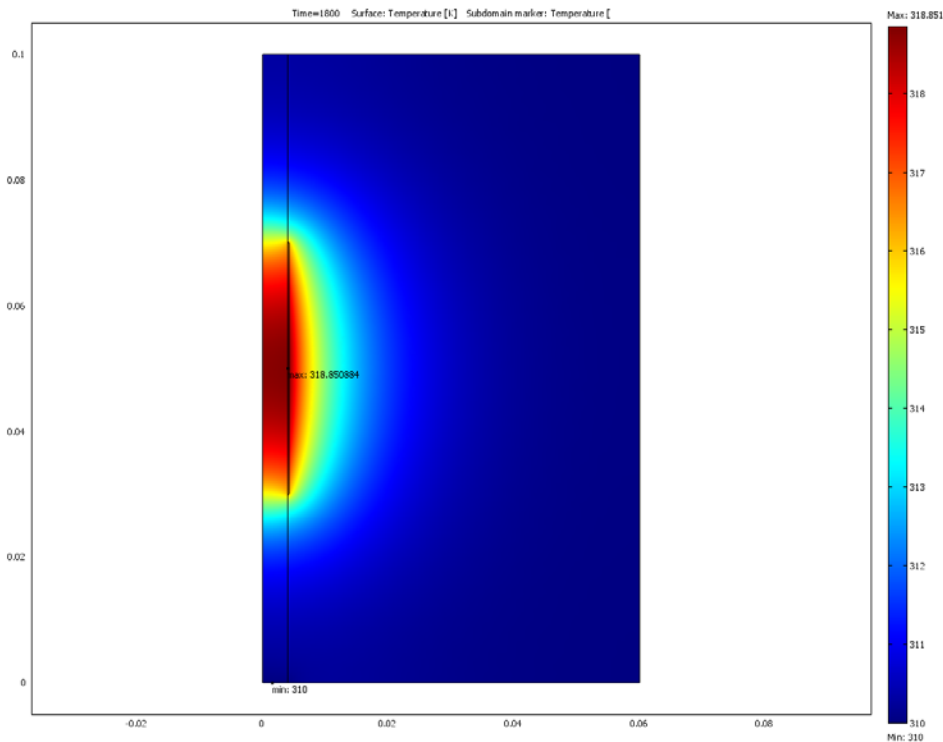
**Figure 14.** Average model temperature after 30 minutes of heating over the number of elements in mesh.

Figure 14 implies that the solution is converged across all meshes as there is little or no change in average temperature for any of the models as the number of mesh elements increases.

Figures 2-5 display the temperature surface plots for four models after 30 minutes of heating. Only the large stent without blood perfusion reached a maximum temperature in excess of 45°C (318K). The models of the small and large stent with blood perfusion produced maximum temperatures of 310.230 K and 310.807 K respectively after 30 minutes of heating (Figures 2 and 4). The initial temperature of the tissue and the temperature of the blood at the inlet of the artery were set at body temperature or 310 K (Appendix A). Our simulations show that when the cooling effects of blood flow are present, the maximum temperature reached in our model is well under the tissue damage limits. In fact, the temperature rise in the tissue is well under 1°C for both stents. In the

models of a small and a large stent without blood perfusion, maximum temperatures of 312.297K and 318.851K respectively, were reached after 30 minutes of heating. The maximum temperature of the large stent without blood flow did exceed the critical temperature for tissue damage and thus a stent of this size may pose a risk to a patient's health during MRI. However, it is reasonable to assume that a complete lack of blood flow is improbable, even in a patient experiencing restenosis. Furthermore, the extent of reduction in a patient's blood flow could probably be determined in less than 30 minutes of MRI and decisions regarding the advisability of an MRI procedure could then be made.

Figures 6-9 likewise illustrate the change in temperature over time at a coordinate in each of the models. In each case, the coordinate chosen is very near the position where maximum temperature is reached after 30 minutes of heating. These graphs imply that while the temperature profiles of the stents with blood perfusion converge over extended time, those of the stents without blood perfusion continue to increase, eventually resulting in tissue damage. Again, complete lack of blood flow is not a realistic scenario and it is likely that even in the case of restenosis some cooling would still take place. Therefore, it is probable that even the large stent does not pose a threat to a patient during MRI since the true solutions for this stent would lie in between our solutions with and without blood perfusion.



**Figure 2.** Temperature surface plot of the model of a large stent without blood perfusion after 30 minutes of heating in MRI.

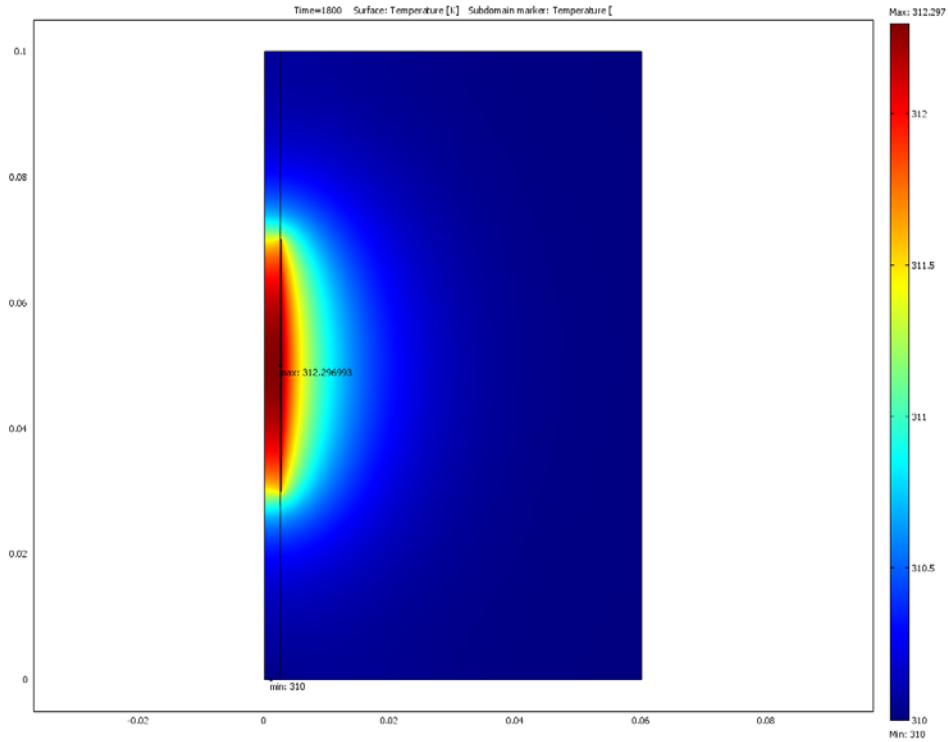


**Figure 3.** Temperature surface plot of the model of a small stent without blood perfusion after 30 minutes of heating in MRI.

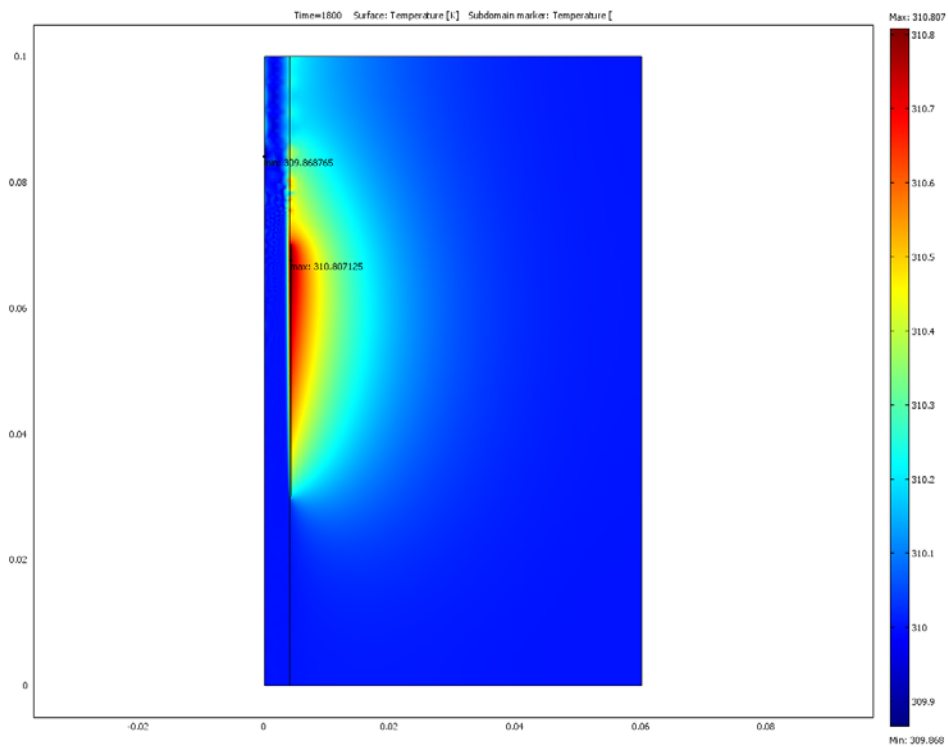


**Figure 4.** Temperature surface plot of the model of a large stent with blood perfusion after 30 minutes of heating in MRI.

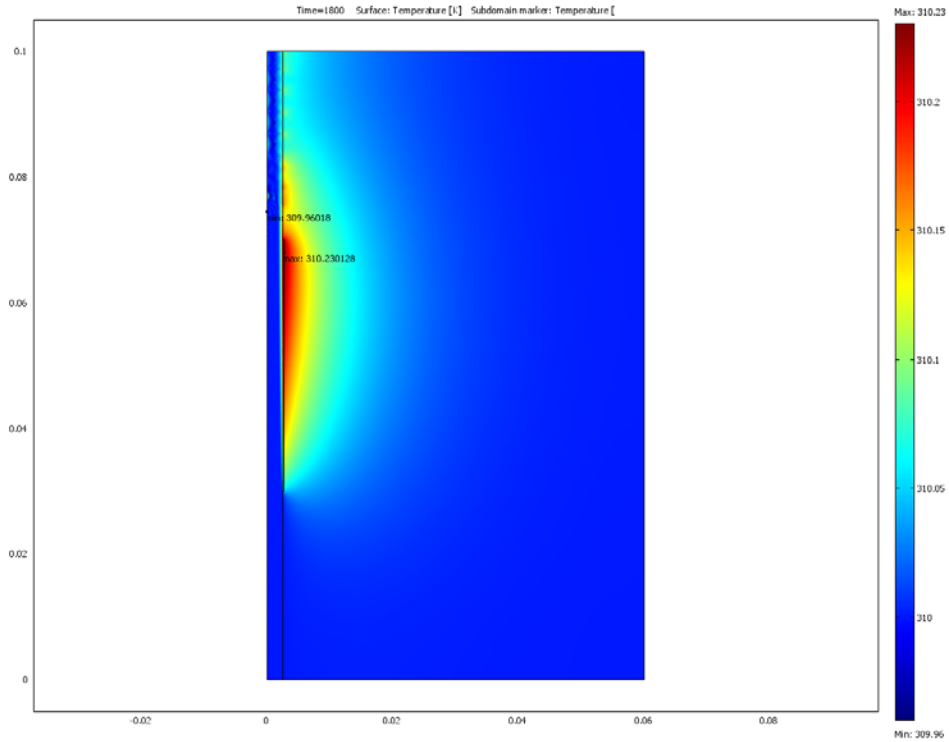


**Figure 5.** Temperature surface plot of the model of a small stent with blood perfusion after 30 minutes of heating in MRI.

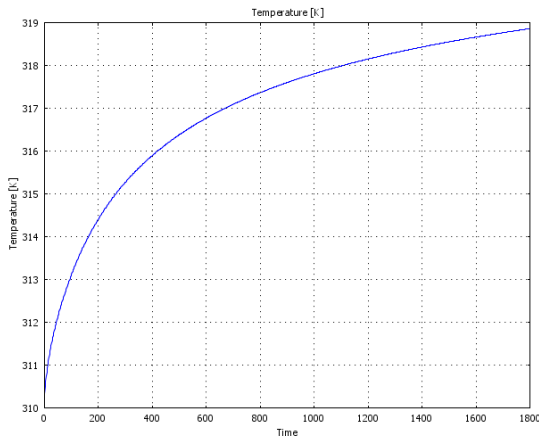


**Figure 6.** Temperature over time (seconds) for position  $[r=0.004\text{m}, z=0.05\text{m}]$  in the model of a large stent without blood perfusion

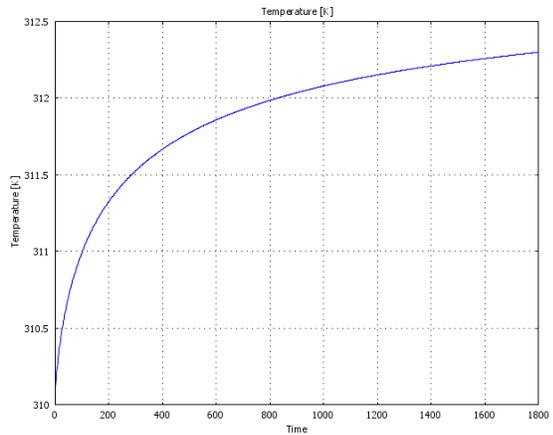


**Figure 7.** Temperature over time (seconds) for position  $[r=0.0025\text{m}, z=0.05\text{m}]$  in the model of a small stent without blood perfusion.

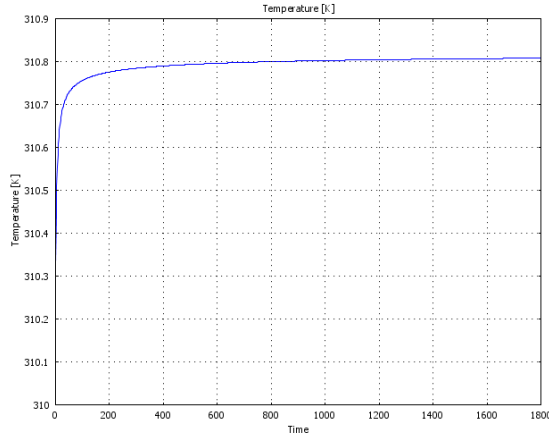


**Figure 8. Temperature over time (seconds) for position  $[r=0.004193\text{m}, z=0.067593\text{m}]$  in the model of a large stent with blood perfusion.**

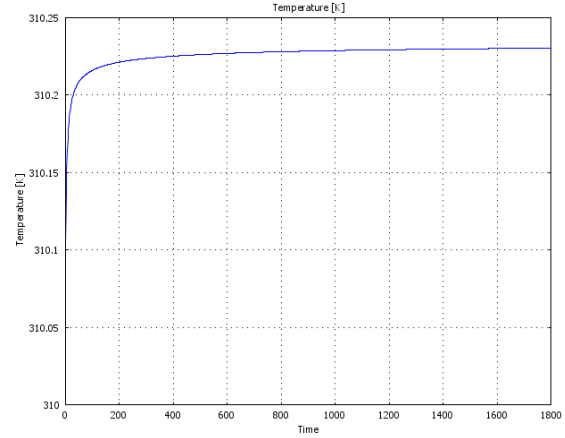


**Figure 9. Temperature over time (seconds) for position  $[r=0.002643\text{m}, z=0.068021\text{m}]$  in the model of a small stent with blood perfusion.**

### 3.2 Sensitivity Analysis

In testing the sensitivity of our models to material property variations, we considered maximum temperature to be a reliable indicator of systemic changes. The various material characteristics were increased or decreased by 10% of the corresponding original values. 10% was used because the standard deviations for each of the constants were unavailable in literature. If standard deviations ( $\sigma$ ) were available, each constant would be varied by  $\pm 3\sigma$  to incorporate 99.7% of the possible values of each constant (assuming normal distribution). The properties tested were those presenting greatest uncertainty in literature and those that did not have a large safety factor built in. These properties included the dynamic viscosity of blood ( $\eta$ ), the electrical conductivity of the metal stent ( $\sigma$ ), the thermal conductivity of the blood and tissue ( $k_{\text{blood}}$  and  $k_{\text{tissue}}$ ), the heat capacity of the blood and tissue ( $c_{\text{blood}}$  and  $c_{\text{tissue}}$ ), the fractional area coverage of the stent ( $\phi$ ), and the densities of blood, tissue, and the stent ( $\rho_{\text{blood}}$ ,  $\rho_{\text{tiss}}$ , and  $\rho_{\text{stent}}$ ). Figures 10-13 show the effects of varying each of these properties in the four models we studied on the final maximum temperature reached after 30 minutes. As Figures 10-13 illustrate, the models with and without blood flow were all very sensitive to variations in electrical conductivity of the stent ( $\sigma$ ) and the fractional area coverage of the stent ( $\phi$ ). This comes as no surprise since both of these terms appear prominently in the equation for the heating of the stent (Equation 1). Increase in either of these terms leads to increased heating and therefore higher maximum temperature after 30 minutes. The models without blood perfusion were also quite sensitive to variations in the physical properties of tissue ( $k_{\text{tissue}}$ ,  $c_{\text{tissue}}$ , and  $\rho_{\text{tiss}}$ ). This is because the heat generated in the stent is primarily removed by conduction through the surrounding tissue. By contrast, the models with blood perfusion were sensitive to variations in the physical properties of blood ( $k_{\text{blood}}$ ,  $c_{\text{blood}}$ , and  $\rho_{\text{blood}}$ ). This is because convection in the blood flow is the primary mechanism of heat removal in these models. Thermal conductivity, heat capacity, and density all appear prominently in the governing equation for heat conduction and convection (Appendix A), so it makes sense that the models would be sensitive to changes in these constants. Variation in the dynamic viscosity of blood ( $\eta$ )

had minimal effect on the final maximum temperature after 30 minutes, suggesting that our models are not very sensitive to this property.

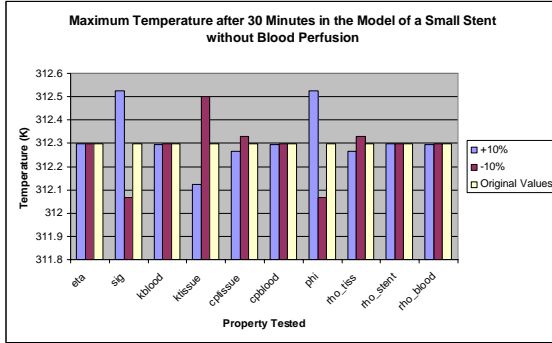


Figure 10.

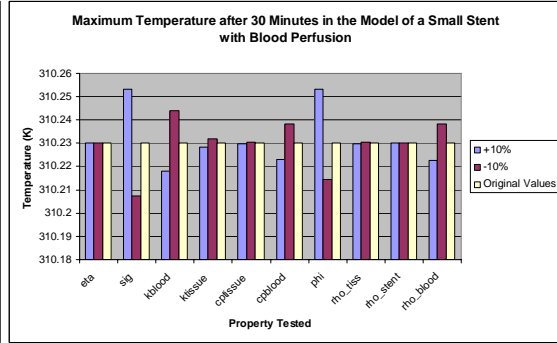


Figure 11.

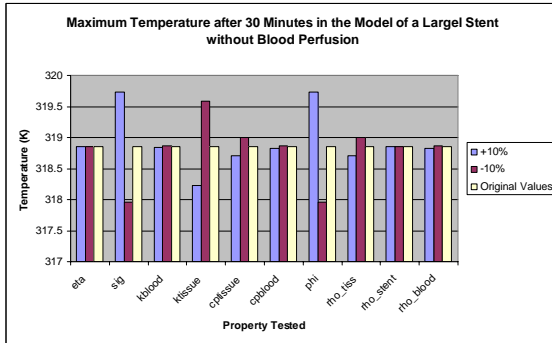


Figure 12.

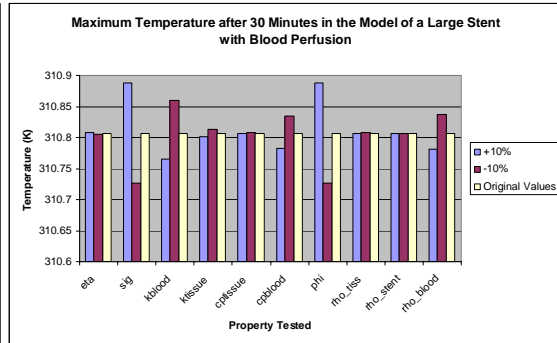


Figure 13.

To calculate total possible error in maximum temperatures after  $\pm 10\%$  variation in each of the material properties described above, we applied the formula in Equation 2, where  $T_{kx}$  is the final maximum temperature when material property  $kx$  is given its original value, and  $T_{kx^*}$  is the final maximum temperature when material property  $kx$  is varied by 10%.

$$Total\ Error\ \Delta T \approx \sqrt{\sum_{kx=eta, sig, k_{blood} \dots} (T_{kx} - T_{kx^*})^2} \quad (Equation\ 2)$$

The total errors in the maximum temperatures for the four models after 30 minutes of heating are summarized in Table 2.

Table 2. Errors in maximum temperatures after 30 minutes of heating

Model	Total Error (K)	Maximum Temperature (K)
Large Stent without Blood Perfusion	1.465	318.851 $\pm$ 1.465
Small Stent without Blood Perfusion	0.387	312.297 $\pm$ 0.387
Large Stent with Blood Perfusion	0.131	310.807 $\pm$ 0.131
Small Stent with Blood Perfusion	0.033	310.230 $\pm$ 0.033

### **3.3 Results Compared with Expected Results**

Similar studies on MRI heating of medical implants, suggest that maximum temperature fluctuations are close to those obtained in our simulations. In one study, for example, researchers exposed 6 and 25 mm stents to heating under industrial furnaces operating at 6.25 or 92.6 kHz. Temperature rise was then estimated based on the time needed for coagulation of egg yolk surrounding the stent. Based on this apparatus, the study reported a maximum temperature rise of 1.1°C without the cooling effects of blood flow.<sup>7</sup> Similar elevations in temperature were also obtained in studies of cervical fixation devices, which are similar metallic implants.<sup>13,14</sup>

The higher temperatures obtained in our non blood flow models are due to the safety factors included in our calculations, the assumptions made in modeling, and the rather long 30 minute heating period used. When blood perfusion was considered, temperature rises were below the 1.1°C value found in literature even with the variation of material properties.

## **4. Conclusions and Design Recommendations**

### **4.1 Conclusion**

Based on these simulations and the assumption that blood flow in a stented artery will never be fully restricted, it is safe to say that 316L stainless steel stents are safe for use in an MR environment. It was already understood that this type of stent is not ferromagnetic and poses no risk of movement in the magnetic fields used in MRI. The present study then confirmed that any risk stemming from heating due to induced currents is also negligible. It suffices to say that even patients inflicted with restenosis will experience heating that lies somewhere in between our blood flow and non blood flow models. Thus the temperatures should remain well below the critical 45°C required to cause tissue damage. For further safety, techniques such as ultrasound employing Doppler shift can be used to quantify blood flow in an artery help evaluate MRI safety. Ultimately, if appropriate precautions are taken, our simulations indicate that a 316L stainless steel wire mesh stent is MR safe.

### **4.2 Realistic Constraints**

A number of simplifications were employed in our study in order to ease the modeling process and provide a safety factor. By modeling all subdomains as cylinders, we achieved the symmetry necessary to create a 2 dimensional axis-symmetric model, a type easily specified in COMSOL. We also assumed a semi-infinite geometry in order to improve our ease of modeling.

Simplifications that acted as safety factors in our solutions were the assumption that the average blood velocity in the artery was the average diastolic velocity from literature; the assumption that our stent is aligned parallel with the RF field in an MRI environment; and the use of maximum values for the amplitude of the RF magnetic field and the

fraction of time that it is applied. These assumptions all contribute to greater heating than what may occur in a realistic situation.

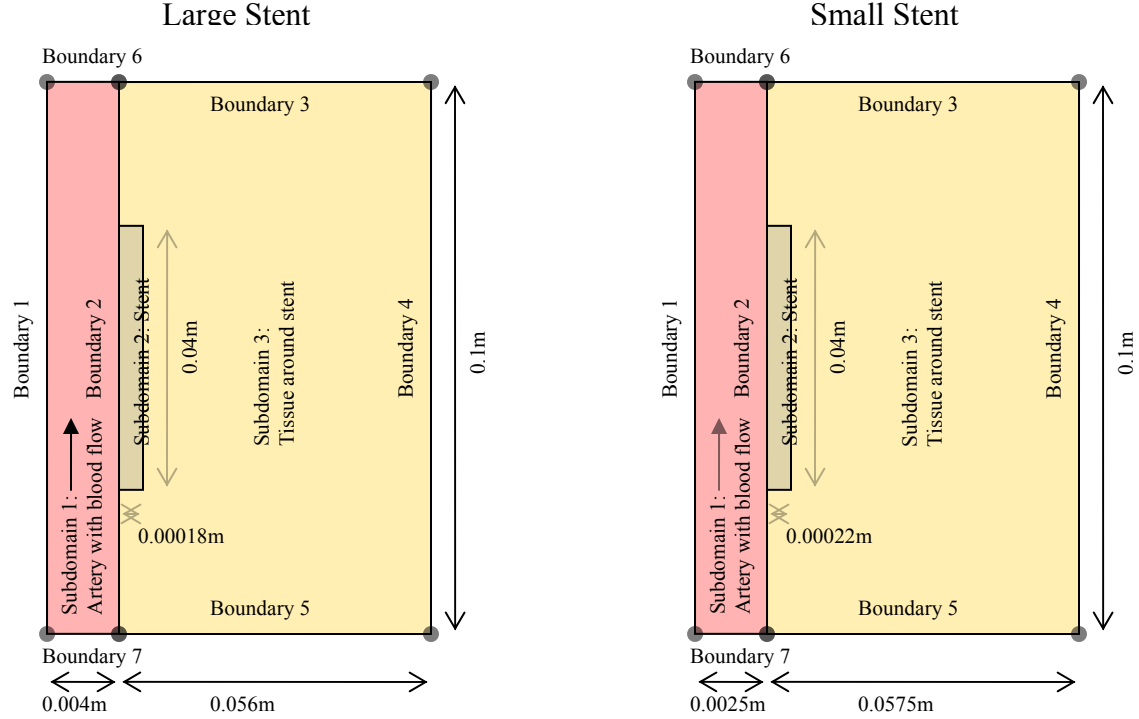
### **4.3 Design Recommendations**

A number of steps could be taken to further reduce the risk that a metallic wire mesh stent poses during MRI. As previously mentioned, other medical techniques could be used to evaluate blood flow through a stent before exposure to an MR environment. Another way to minimize the risk of heating is to construct stents from materials with lower electrical conductivity values. For instance, some titanium alloys already used in medical implants have electrical conductivities that are over an order of magnitude below that of 316L stainless steel ( $1.3 \cdot 10^6$  S/m). The problem of heating could be eliminated entirely if a nonconductive material were used. However, metals are the primary materials used in stent construction because of their material properties.

## 5. Appendices

### Appendix A – Model Physics

#### A.1 Geometry and Schematic



#### A.2 Governing Equations

Navier Stokes Equation: Cylindrical Geometry  
Applied in Subdomain 1 (Artery) of models with blood perfusion

$$\rho \left( \frac{\partial v_\theta}{\partial t} + v_r \frac{\partial v_\theta}{\partial r} + \frac{v_\theta \partial v_\theta}{r \partial \theta} + \frac{v_r v_\theta}{r} + v_z \frac{\partial v_\theta}{\partial z} \right) = -\frac{1}{r} \frac{\partial p}{\partial \theta} + \rho g_\theta + \mu \left[ \frac{1}{r} \frac{\partial}{\partial r} \left( r \frac{\partial v_\theta}{\partial r} \right) - \frac{v_\theta}{r^2} + \frac{1}{r^2} \frac{\partial^2 v_\theta}{\partial \theta^2} + \frac{2}{r^2} \frac{\partial v_r}{\partial \theta} + \frac{\partial^2 v_\theta}{\partial z^2} \right]$$

$$\rho \left( \frac{\partial v_r}{\partial t} + v_r \frac{\partial v_r}{\partial r} + \frac{v_\theta \partial v_r}{r \partial \theta} - \frac{v_\theta^2}{r} + v_z \frac{\partial v_r}{\partial z} \right) = -\frac{\partial p}{\partial r} + \rho g_r + \mu \left[ \frac{1}{r} \frac{\partial}{\partial r} \left( r \frac{\partial v_r}{\partial r} \right) - \frac{v_r}{r^2} + \frac{1}{r^2} \frac{\partial^2 v_r}{\partial \theta^2} - \frac{2}{r^2} \frac{\partial v_\theta}{\partial \theta} + \frac{\partial^2 v_r}{\partial z^2} \right]$$

$$\rho \left( \frac{\partial v_z}{\partial t} + v_r \frac{\partial v_z}{\partial r} + \frac{v_\theta \partial v_z}{r \partial \theta} + v_z \frac{\partial v_z}{\partial z} \right) = -\frac{\partial p}{\partial z} + \rho g_z + \mu \left[ \frac{1}{r} \frac{\partial}{\partial r} \left( r \frac{\partial v_z}{\partial r} \right) + \frac{1}{r^2} \frac{\partial^2 v_z}{\partial \theta^2} + \frac{\partial^2 v_z}{\partial z^2} \right]$$

Due to symmetry in the theta direction, all the theta terms in the above equations drop out.

Conduction Equation: Cylindrical Geometry  
Applied throughout the models

$$\rho c_p \frac{\partial T}{\partial t} = k \left( \frac{1}{r} \frac{\partial}{\partial r} \left( r \frac{\partial T}{\partial r} \right) + \frac{1}{r^2} \left( \frac{\partial^2 T}{\partial \phi^2} \right) + \frac{\partial^2 T}{\partial z^2} \right) + Q$$

### A.3 Initial and Boundary Conditions

See A.1 for Subdomains and Boundaries. All boundaries not specified here were solved for by the computer during simulation.

#### A.3.1 Boundary Conditions – Models without Blood Perfusion

Heat Conduction:

Boundary 1:  $\frac{\partial T}{\partial x} = 0$  Zero heat flux, axial symmetry.

Boundary 3-7:  $\frac{\partial T}{\partial x} = 0$  Zero heat flux, semi-infinite geometry.

#### A.3.2 Boundary Conditions – Models with Blood Perfusion

Heat Conduction:

Boundary 1:  $\frac{\partial T}{\partial x} = 0$  Zero heat flux, axial symmetry.

Boundary 3-5:  $\frac{\partial T}{\partial x} = 0$  Zero heat flux, semi-infinite geometry.

Boundary 6: Bulk flow convective flux condition. COMSOL removes heat from the model due to bulk flow of blood in the artery.

Boundary 7:  $T = 310K$  Constant temperature of blood inflow.

Navier-Stokes:

Boundary 1:  $r = 0$  Slip boundary condition, axial symmetry. Not a true boundary.

Boundary 2:  $u = 0$  No slip boundary condition.

Boundary 6:  $p = 0$  No pressure, normal flow condition.

Boundary 7:  $u = 0.15m/s$  Average blood velocity, inflow velocity.

#### A.3.3 Initial Conditions – Models without Blood Perfusion

Heat Conduction:

Subdomain 1-3:  $T = 310K$  Initial temperature at body temperature throughout.

#### A.3.4 Initial Conditions – Models with Blood Perfusion

Heat Conduction:

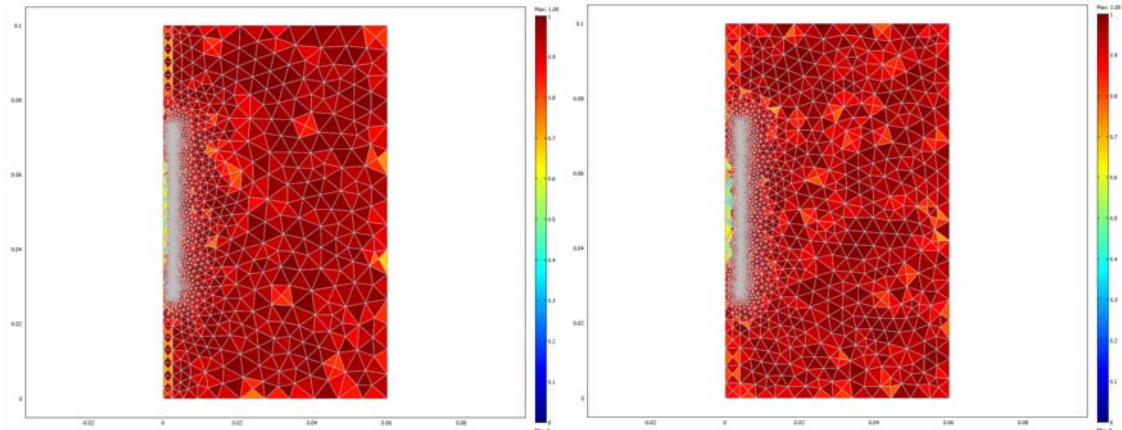
Subdomain 1-3:  $T = 310K$  Initial temperature at body temperature throughout.

Navier-Stokes:

Subdomain 1:  $u = 0$  No flow initially.

Subdomain 2-3: Not included in modeling fluid flow.

#### A.4 Meshes Used



Small Stent: 6287 Elements

Large Stent: 5146 Elements

#### Appendix B – Solution Details and Model Reports

The following model report was generated for the model of a small stent with blood perfusion. The other models were identical to this in terms of solver used, tolerances applied, and constants, with the exception of the stent dimensions.



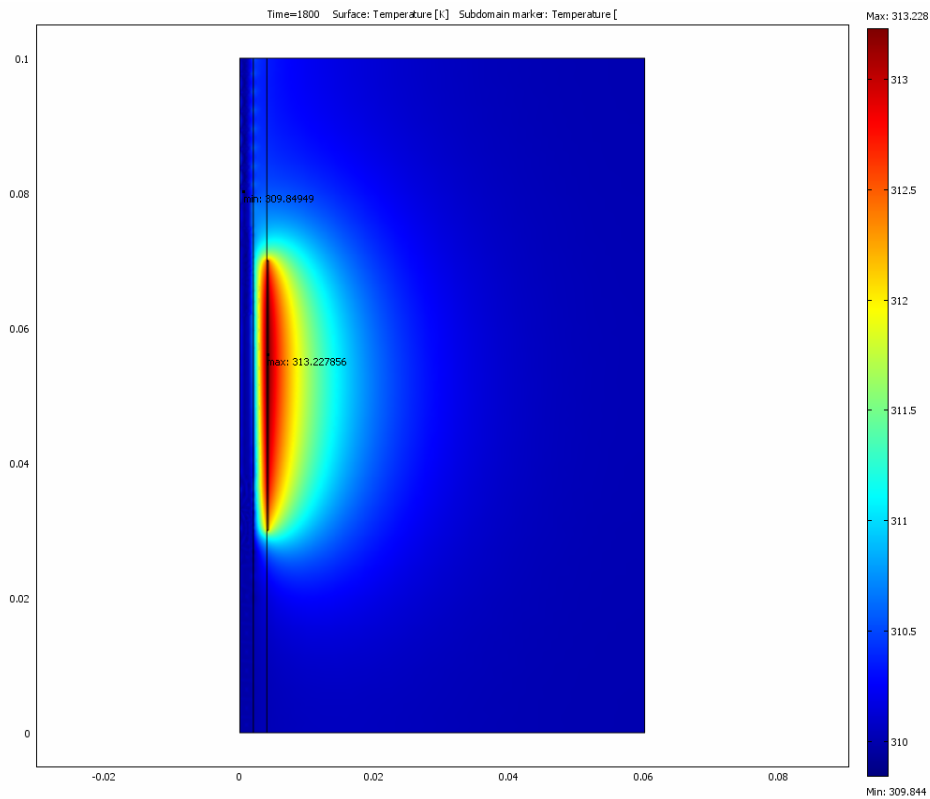


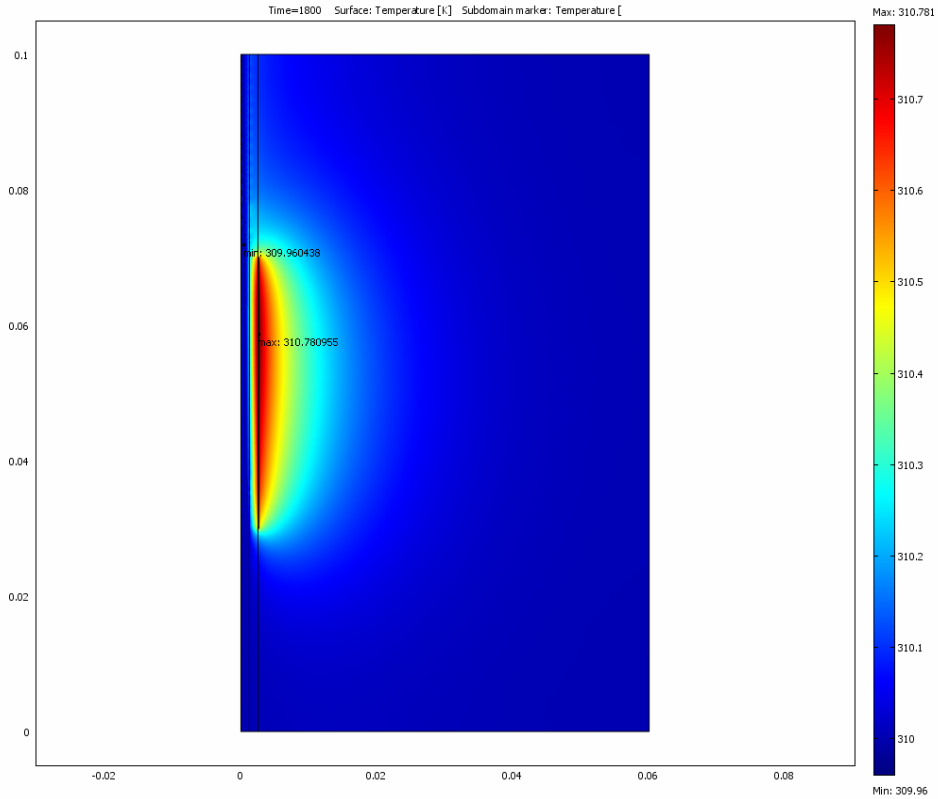




## Appendix C – Further Simulation

In an effort to demonstrate our assertion that in a realistic situation, the model for heating of a stent in a patient experiencing restenosis would lie in between our solutions for models with and without blood perfusion, we created duplicates of our models of a small and large stent with blood perfusion. In these models, we reduced the artery diameter by a factor of 2 by inserting a tissue layer on the inside of the stent. This layer was given the same physical properties as the tissue surrounding the stent. The arterial blood velocity and dynamic viscosity of blood remained the same as in our previous models. The following surface plots illustrate the results of 30 minutes of heating in these new models and document the maximum temperatures reached. In both models, these maximum temperatures are well below the temperature at which tissue damage occurs.





**Small Stent - Restenosis**

The following charts also illustrate temperature rise over time for a point in each of the models near the point where maximum temperature rise after 30 minutes occurs. These charts indicate that while the total temperature rise is higher than in the models with unobstructed blood flow, the solution does converge over extended time and is closer to the models previously generated with blood perfusion than those without.

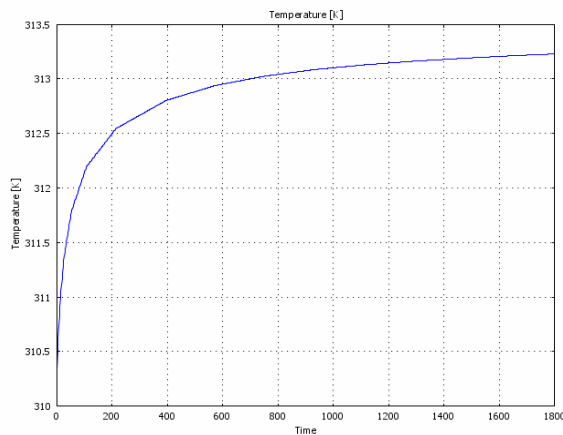


**Figure 8. Temperature over time (seconds) for position  $[r=0.004143\text{m}, z=0.056069\text{m}]$  in the model of a large stent with restenosis.**

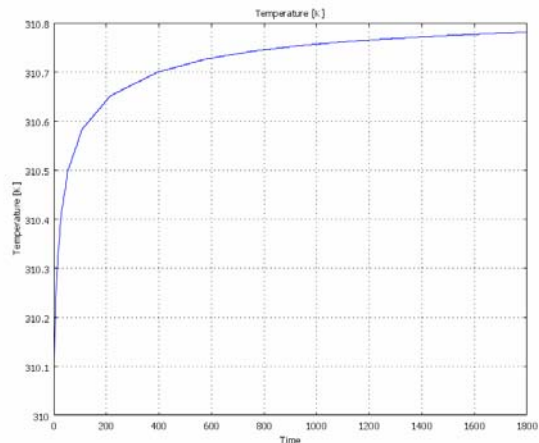


**Figure 9. Temperature over time (seconds) for position  $[r=0.002606\text{m}, z=0.059607\text{m}]$  in the model of a small stent with restenosis.**

## Appendix D – References

- <sup>1</sup>Bartels, L. W., Smits, H. F. M., Bakker, C. J. G., Viergever, M. A. 2001. *MR Imaging of Vascular Stents: Effects of Susceptibility, Flow, and Radiofrequency Eddy Currents. Journal of Vascular Interventional Radiology.* 12:365-371.
- <sup>2</sup>Berry, I., Barker, G. J., Barkhof, F., Campi, A., Dousset, V., Franconi, J., Gass, A., Schreiber, W., Miller, D. H., Tofts, P. S. 1999. *A Multicenter Measurement of Magnetization Transfer Ratio in Normal White Matter. Journal of Magnetic Resonance Imaging.* 9:441-446.
- <sup>3</sup>Busch, M. H. J., Vollmann, W., Schnorr, J., Grönemeyer, D. H. W. 2005. *Finite volume analysis of temperature effects induced by active MRI implants with cylindrical symmetry: 1. Properly working devices. Biomedical Engineering Online.* 4:25.
- <sup>4</sup>Busch, M. H. J., Vollmann, W., Schnorr, J., Grönemeyer, D. H. W. 2005. *Finite volume analysis of temperature effects induced by active MRI implants with cylindrical symmetry: 2. Defects on active MRI implants causing hot spots. Biomedical Engineering Online.* 5:35.
- <sup>5</sup>Collins, C. M., Smith, M. B. 2001. *Calculations of  $B_1$  Distribution, SNR, and SAR for a Surface Coil Adjacent to an Anatomically-Accurate Human Body Model. Magnetic Resonance in Medicine.* 45:692-699.
- <sup>6</sup>Davis, P. L., Crooks, L., Arakawa, M., McRee, R., Kaufman, L., Margulis, A. R., 1981. *Potential Hazards in NMR Imaging: Heating Effects of Changing Magnetic Fields and RF Fields on Small Metallic Implants. American Journal of Roentgenology.* 137:857-860.
- <sup>7</sup>Foster, Kenneth R., Goldberg, R., Bonsignore, C. 1999. *Heating of Cardiovascular Stents in Intense Radiofrequency Magnetic Fields. Bioelectromagnetics.* 20:112-116.
- <sup>8</sup>Ho, H. S. 2001. *Safety of Metallic Implants in Magnetic Resonance Imaging. Journal of Magnetic Resonance Imaging.* 14:472-477
- <sup>9</sup>Holton, A., Walsh, E., Anayiotos, A., Pohost, G., Venugopalan, R. 2002. *Comparative MRI Compatibility of 316L Stainless Steel Alloy and Nickel-Titanium Alloy Stents. Journal of Cardiovascular Magnetic Resonance.* 4(4):423-430
- <sup>10</sup>Hug, J., Nagel, E., Bornstedt, A., Schnackenburg, B., Oswald, H., Fleck, E. 2000. *Coronary Arterial Stents: Safety and Artifacts during MR Imaging. Radiology.* 216:781-787.
- <sup>11</sup>Müller, G. J., Roggam, A. 1995. *Laser-induced interstitial thermotherapy.* SPIE Optical Engineering Press, Bellingham, Wash.

- <sup>12</sup>Rosenson, Robert S., McCormick, A., Uretz, Eugene F. 1996. *Distribution of blood viscosity values and biochemical correlates in health adults. Clinical Chemistry.* 42(8):1189-1195.
- <sup>13</sup>Shellock, Frank G. 1996. *MR Imaging and Cervical Fixation Devices: Evaluation of Ferromagnetism, Heating, and Artifacts at 1.5 Tesla. Magnetic Resonance Imaging.* 14(9): 1093-1098.
- <sup>14</sup>Shellock, Frank G., Cosendai, G., Park, S., Nyenhuis, J. A. 2004. *Implantable Microstimulator: Magnetic Resonance Safety at 1.5 Tesla. Investigative Radiology.* 39(10):591-599.
- <sup>15</sup>Tofts, Paul S. Letter to the authors. 16 Mar. 2007.
- <sup>16</sup>United States. U.S. Department of Health and Human Services: Food and Drug Administration Center for Devices and Radiological Health. *A Primer on Medical Device Interactions with Magnetic Resonance Imaging Systems.* 1997. <<http://www.fda.gov/cdrh/ode/primerf6.html>>.
- <sup>17</sup>Yildirim, A., Soylu, O., Dagdeviren, B., Ergelen, M., Celik, S., Zencirci, E., Tezel, T. 2007. *Cardiac Resynchronization Improves Coronary Blood Flow. Tohoku Journal of Experimental Medicine.* 211:43-47.